Cell

Graded Expression of Semaphorin-1a Cell-Autonomously Directs Dendritic Targeting of Olfactory Projection Neurons

Takaki Komiyama,[1,3] Lora B. Sweeney,[1] Oren Schuldiner,[1] K. Christopher Garcia,[2] and Liqun Luo[1,*]
[1] Department of Biological Sciences and Neurosciences Program
[2] Department of Molecular and Cellular Physiology
Howard Hughes Medical Institute, Stanford University, Stanford, CA 94305, USA
[3] Present address: Janelia Farm Research Campus, Howard Hughes Medical Institute, Ashburn, VA 20147, USA.
*Correspondence: lluo@stanford.edu
DOI 10.1016/j.cell.2006.12.028

SUMMARY

Gradients of axon guidance molecules instruct the formation of continuous neural maps, such as the retinotopic map in the vertebrate visual system. Here we show that molecular gradients can also instruct the formation of a discrete neural map. In the fly olfactory system, axons of 50 classes of olfactory receptor neurons (ORNs) and dendrites of 50 classes of projection neurons (PNs) form one-to-one connections at discrete units called glomeruli. We provide expression, loss- and gain-of-function data to demonstrate that the levels of transmembrane Semaphorin-1a (Sema-1a), acting cell-autonomously as a receptor or part of a receptor complex, direct the dendritic targeting of PNs along the dorsolateral to ventromedial axis of the antennal lobe. Sema-1a also regulates PN axon targeting in higher olfactory centers. Thus, graded expression of Sema-1a contributes to connection specificity from ORNs to PNs and then to higher brain centers, ensuring proper representation of olfactory information in the brain.

INTRODUCTION

Spatial representation of the external world is a common feature of sensory systems. The visual, auditory, and somatosensory systems are represented in continuous and topographic maps, where neighboring sensory inputs map to neighboring areas in the brain. This organization fits well with the continuous nature of these sensory stimuli, since visual and somatosensory stimuli are spatially continuous and auditory stimuli have continuous frequencies. By contrast, the olfactory system, whose main goal is to identify the quality of olfactory stimuli, utilizes a different strategy. The antennal lobe/olfactory bulb, the first olfactory relay in the brain, is composed of discrete units called glomeruli. In each glomerulus, axons of olfactory receptor neurons (ORNs) of a single class that express the same olfactory receptor converge and synapse typically with a single class of uniglomerular projection neurons (PNs)/mitral cells. Thus, odor information is organized in a discrete spatial map in the brain, which consists of discrete glomerular units (reviewed in Axel, 1995; Komiyama and Luo, 2006). The mechanisms by which continuous maps develop have been extensively studied in the visual system and shown to utilize gradients of guidance molecules (reviewed in McLaughlin and O'Leary, 2005; Flanagan, 2006). By contrast, relatively little is known about mechanisms by which discrete sensory maps exemplified by the olfactory system are constructed (Komiyama and Luo, 2006). Do continuous and discrete sensory maps develop using qualitatively different strategies, or are there commonalities?

At the antennal lobe of the adult fly olfactory system, axons of 50 classes of ORNs and dendrites of 50 classes of second-order PNs form one-to-one connections at 50 stereotyped glomeruli (Laissue et al., 1999; Couto et al., 2005; Fishilevich and Vosshall, 2005). Glomerular targeting of PN dendrites is prespecified by their lineage and birth order (Jefferis et al., 2001). Indeed, the initial dendritic targeting of PNs in the antennal lobe occurs prior to invasion of ORN axons (Jefferis et al., 2004) and is regulated by the intrinsic action of transcription factors (Komiyama et al., 2003; Komiyama and Luo, 2007). This provides an excellent opportunity to study mechanisms of active dendritic targeting during the construction of a neural map. To date, however, the cell biological mechanisms by which individual PN classes target their dendrites to distinct positions of the antennal lobe are not understood. Genetic analyses of candidate cell-surface molecules such as N-cadherin and Dscam have revealed their respective functions in restricting dendritic targeting to single glomeruli and in dendritic elaboration within individual glomeruli (Zhu and Luo, 2004; Zhu et al., 2006). Since mutations of N-cadherin and Dscam

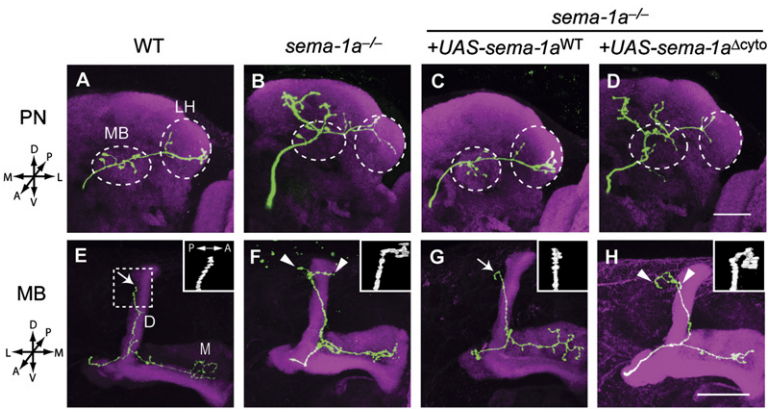

Figure 1. Sema-1a as a Receptor for Axon Targeting

(A) Wild-type (WT) DL1 PN axons terminate in the two outlined structures, the calyx of the mushroom body (MB) and the lateral horn (LH).

(B) *sema-1a*$^{-/-}$ axons mistarget outside these structures (n = 14/14).

(C and D) *sema-1a*$^{-/-}$ axon mistargeting phenotype is rescued by a transgene encoding full-length Sema-1a (C; n = 8/8), but not by a variant that lacks the entire cytoplasmic domain (D; n = 8/8).

(E) Each α'/β' MB neuron has two major axon branches, dorsal (D) and medial (M). WT dorsal axons terminate to a specific region without branching (arrow, n = 39/40).

(F) *sema-1a*$^{-/-}$ axons exhibit multiple branches at the dorsal terminus, which extend beyond the normal α'/β' axon lobe in both M-L axis (arrowheads) and in A-P axis (inset) (n = 14/14).

(G and H) *sema-1a*$^{-/-}$ axon mistargeting phenotype in MB α'/β' neuron is rescued by a transgene encoding full-length Sema-1a (G; n = 23/25), but not by a variant that lacks the entire cytoplasmic domain (H; n = 23/27). Insets are 3D rendering of the dorsal axon tips (dashed boxes) rotated by 90° around the D-V axis.

Unless otherwise mentioned, in this and all subsequent figures, green staining is for mCD8-GFP marking MARCM clones (all clones shown in this figure are single cell clones), and magenta represents synaptic marker nc82 staining. Magenta in (E–H) represents anti-FasII staining, which labels γ and α/β but not α'/β' MB neurons (Lee et al., 1999). The overlap between green and magenta is a result of Z projection. Scale bar, 40 μm. D: dorsal; V: ventral; L: lateral; M: medial; A: anterior; P: posterior.

affect all PN classes equally, these proteins do not appear to play instructive roles in the selection of dendritic targets of individual PN classes.

In principle, each PN class could express a unique combination of cell-surface receptors, so that the resulting combinatorial code specifies targeting of dendrites to one of 50 positions that eventually develop into 50 discrete glomeruli. Alternatively, analogous to the visual system, gradients of guidance molecules can be used to instruct dendritic targeting along different axes, such that different levels of guidance molecules specify different points along each axis. These two models are not mutually exclusive. Here we provide evidence supporting the second model. We show that the transmembrane Semaphorin-1a (Sema-1a) acts cell-autonomously as a receptor or part of a receptor complex to guide PN dendrites and axons. Different PN classes express different levels of Sema-1a, and Sema-1a levels instruct PN dendritic targeting in the antennal lobe along the dorsolateral-to-ventromedial axis.

RESULTS

Sema-1a as a Receptor for Axon Targeting

Semaphorins are a large conserved family of axon guidance molecules that have been shown to function as ligands for the Plexin/Neuropilin receptors (reviewed in Dickson, 2002). However, the vertebrate transmembrane Sema6D functions as a receptor during cardiac cell migration (Toyofuku et al., 2004). Similarly, Sema4D likely functions as a receptor in the immune system (Kumanogoh and Kikutani, 2004). Do transmembrane semaphorins also function cell-autonomously as axon guidance receptors in the nervous system? This possibility has been proposed in a number of reports (Eckhardt et al., 1997; Klostermann et al., 2000; Leighton et al., 2001; Godenschwege et al., 2002), and was shown to be the case for *Drosophila* Sema-1a in photoreceptor axon targeting (Cafferty et al., 2006). Below we provide evidence that Sema-1a functions as a receptor in axon targeting of PNs and mushroom body (MB) neurons.

Sema-1a is a transmembrane semaphorin (Kolodkin et al., 1993) required for correct pathfinding of embryonic motor neurons (Yu et al., 1998), functioning as a ligand for PlexinA (Winberg et al., 1998). It also controls proper synapse formation in the adult giant fiber system, where Sema-1a can have cell-autonomous effects when overexpressed (Godenschwege et al., 2002). To test whether Sema-1a functions as a receptor for axon guidance, we utilized a protein null allele *sema-1a*^{P1} (Yu et al., 1998) and generated single cell *sema-1a*$^{-/-}$ clones in a heterozygous background using the MARCM system (Lee and Luo, 1999) in PNs, whose dendrites innervate the glomerulus DL1, and in MB α'/β' neurons (Lee et al., 1999). We observed defects in axonal development of *sema-1a*$^{-/-}$ single cell clones of both neuronal types. Wild-type DL1 PN axons have a stereotypical axonal projection pattern, with their termini confined in the MB calyx and the lateral horn (Marin et al., 2002; Wong et al., 2002; Komiyama et al., 2003) (Figure 1A). However, single *sema-1a*$^{-/-}$ DL1 PN axons in a heterozygous background mistargeted out of the correct areas and showed exuberant branching (Figure 1B). This phenotype was rescued by expression of a wild-type Sema-1a transgene (sema-1a^{WT}) only in the labeled single cell (Figure 1C), strictly demonstrating

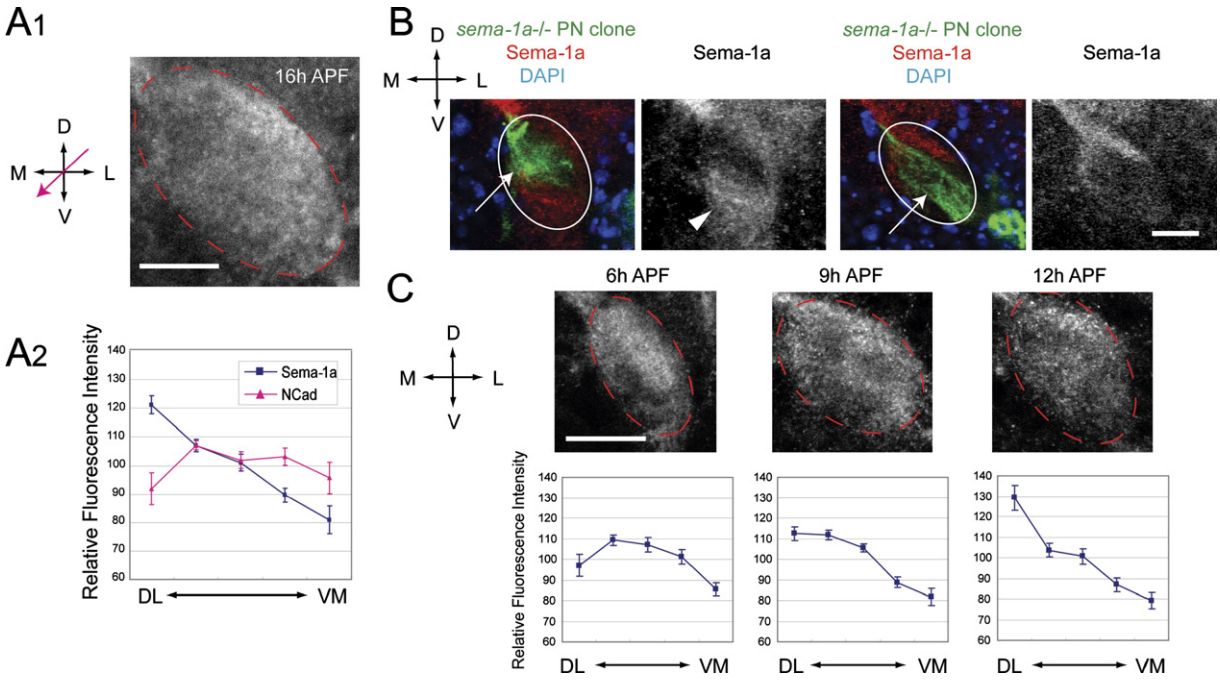

Figure 2. Sema-1a on Projection Neuron Dendrites Forms a Gradient

(A) In (A_1) Sema-1a is distributed in a continuous, high dorsolateral, low ventromedial gradient (following the red arrow) in the antennal lobe (dotted oval) at 16 hr APF. In (A_2) is shown quantification of the Sema-1a gradient (blue, n = 11) and a control protein N-Cadherin (red, n = 9) in the same optical sections. Error bars represent SEM. The relative fluorescence intensity necessarily includes background levels of staining, which differ from brain to brain and does not reflect the absolute steepness of the molecular gradient.

(B) Sema-1a expression (red) is markedly reduced when PNs are *sema-1a*$^{-/-}$ (arrow) in two examples of anterodorsal and lateral double MARCM neuroblast clones (labeled in green) at 18–20 hr APF. Ovals outline the developing antennal lobes. Right panels of each example show Sema-1a staining alone. Careful examination of confocal stacks shows that the Sema-1a signal at the arrowhead is contributed by ORN axons that have started contacting the antennal lobe.

(C) Sema-1a distribution in the antennal lobe during early pupal development (6, 9, and 12 hr APF). Along the DL-VM axis, the gradient becomes steeper and more obvious during this developmental period. Dotted ovals represent developing antennal lobes. At all these time points, the antennal lobes are devoid of cell bodies, and PN cell bodies reside in the periphery of the antennal lobe. Quantified in the bottom panels. N = 12, 11, and 9, for 6, 9, and 12 hr APF, respectively.

Scale bars, 20 μm. Single confocal sections are shown for each panel.

cell-autonomous action of Sema-1a. However, cell-autonomous expression of a transgene lacking the cytoplasmic domain but with intact extracellular and transmembrane domains (sema-1a$^{\Delta cyto}$) failed to rescue the targeting defects (Figure 1D). We have confirmed that Sema-1a$^{\Delta cyto}$ was highly expressed along the entire axon (data not shown), and this truncated protein has been shown to preserve the Sema-1a function as a ligand (Godenschwege et al., 2002). Therefore the cytoplasmic domain of Sema-1a does not appear to be required for localization or surface expression of Sema-1a. Analogous experiments in MB α′/β′ neurons yielded similar results (Figures 1E–1H). These data indicate that Sema-1a functions as a receptor, or part of a receptor complex, in DL1 PNs and MB α′/β′ neurons for axon targeting.

Sema-1a Protein Is Distributed as a Gradient in the Developing Antennal Lobe

Using a polyclonal antibody specific to Sema-1a (Yu et al., 1998; Godenschwege et al., 2002), we found that the Sema-1a protein is distributed in the antennal lobe in a high dorsolateral (DL), low ventromedial (VM) gradient at 16 hr (Figures 2A_1 and A_2, n = 11) and 18 hr (data not shown) after puparium formation (APF). In the anterior-posterior (Z) axis of the antennal lobe, the gradient distribution is most prominent at central-to-posterior sections. The Sema-1a gradient does not arise from a graded density of PN dendrites, since the density of PN dendrites is rather uniform within the antennal lobe at these developmental stages as shown by N-cadherin staining (Figure 2A_2) (Zhu and Luo, 2004). Shortly after 18 hr APF, ORN axons expressing a high level of Sema-1a reach the antennal lobe (Sweeney et al., 2007). As a result, the Sema-1a PN gradient is no longer evident at later time points. Sema-1a is undetectable in the adult antennal lobe (data not shown).

At 16 hr and 18 hr APF, PN dendrites are the major component of the antennal lobe, as ORN axons have not yet entered (Jefferis et al., 2004). In addition, all PN classes previously examined at this stage have targeted their

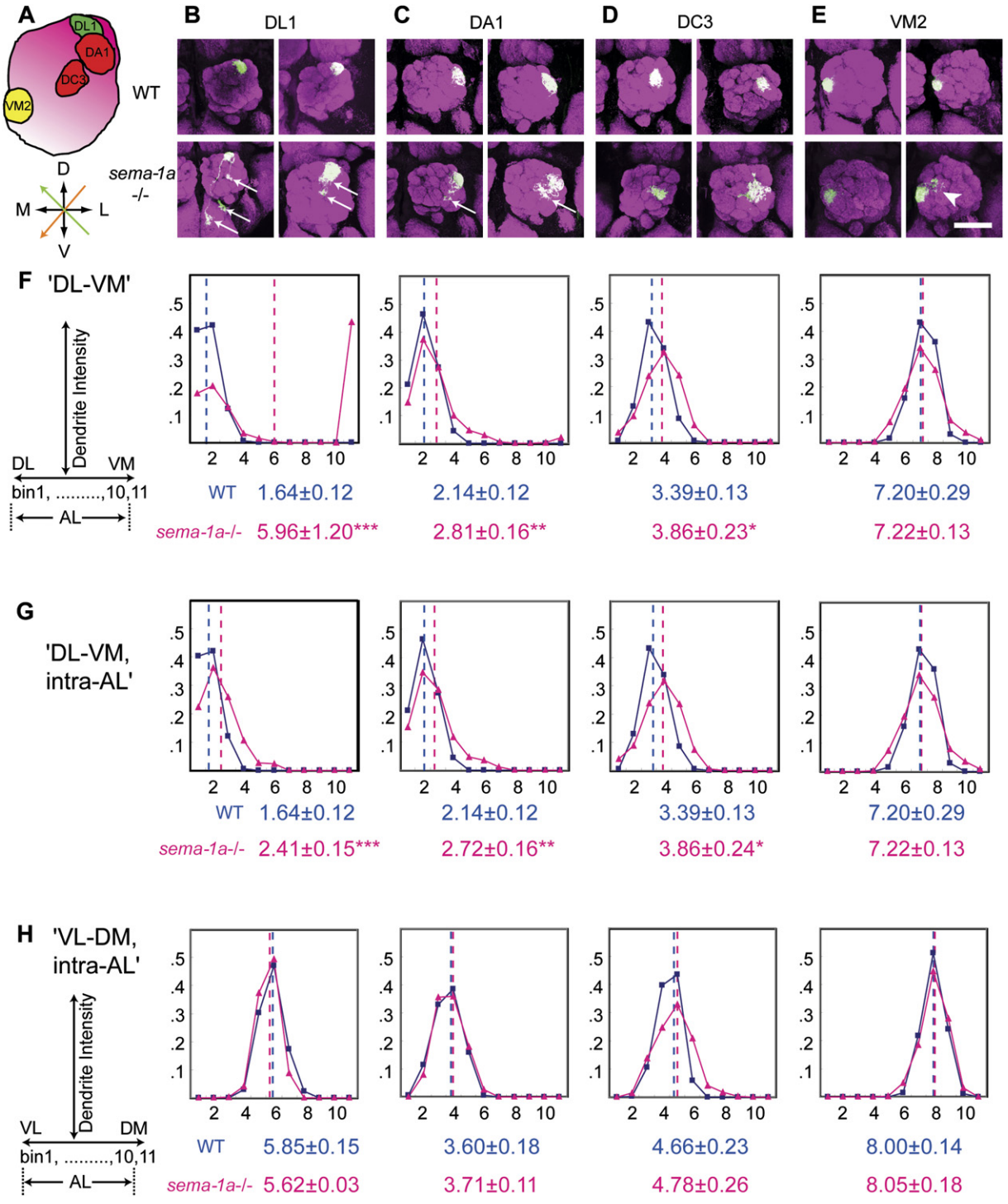

Figure 3. Dendritic Targeting Phenotypes of *sema-1a*$^{-/-}$ Single-Cell Clones

(A) A schematic of the positions of four glomeruli used in this study. Green: GH146-Gal4 (labels invariably the DL1 PN when clones are induced in early larvae); red: MZ19-Gal4 (labels DA1 and DC3 PNs that can be further distinguished based on their neuroblast lineages); yellow: NP5103-Gal4 (labels only VM2 PN).

(B–E) Dendritic targeting of single-cell MARCM clones of a defined class of WT and *sema-1a*$^{-/-}$ PNs. Two examples of each condition are shown. Arrows indicate dendritic mistargeting in *sema-1a*$^{-/-}$ DL1 and DA1 PNs. The arrowhead indicates the occasional mistargeting of *sema-1a*$^{-/-}$ VM2 PNs in the DL direction. Scale bar, 70 μm for the bottom left of (B) and 50 μm for all other panels.

(F) Quantification of dendritic targeting along the DL-VM axis (the orange axis in [A], for details see Figure S1). In short, the antennal lobe is divided into ten bins along the DL-VM axis, with bin1 being the most DL. The relative fluorescence intensity (dendritic density) of single-cell clones within each bin

dendrites to appropriate regions of the antennal lobe according to their future glomerular classes and have a similar dendritic arborization status (Jefferis et al., 2004). Therefore the Sema-1a gradient in the developing antennal lobe suggests that dendrites of different PN classes express different levels of Sema-1a. We provide the following experimental evidence to support this idea. First, when an UAS-RNAi transgene against *sema-1a* was driven by a pan-neuronal elav-Gal4, overall Sema-1a staining of the pupal nervous system including the developing antennal lobe was greatly reduced (Sweeney et al., 2007). This result supports the previous reports that this antibody is specific (Yu et al., 1998; Godenschwege et al., 2002) and shows that Sema-1a expression is mostly neuronal. Second, making a large subset of PNs mutant for *sema-1a* greatly reduced the Sema-1a staining in the antennal lobe. About two-thirds of PNs are labeled by Gal4-GH146 (Stocker et al., 1997), most of which derive from either the anterodorsal or the lateral neuroblast lineages (Jefferis et al., 2001). We can eliminate Sema-1a from individual lineages by generating protein null *sema-1a*$^{-/-}$ MARCM neuroblast clones in a heterozygous background. Rarely we obtained double neuroblast clones such that the majority of GH146-positive PNs (except those born prior to clone generation) are devoid of Sema-1a protein. Figure 2B shows two such examples: a marked reduction of Sema-1a staining was observed coinciding with labeled, mutant PN dendrites. The residual Sema-1a staining could be due to the nonlabeled PNs that are heterozygous for *sema-1a*. Taken together, we conclude that the graded Sema-1a distribution is largely contributed by PN dendrites.

To determine the onset of the Sema-1a gradient during development, we performed immunostaining at earlier pupal stages (Figure 2C). At 6 hr APF, the Sema-1a distribution does not show an obvious uniform gradient. This evolves into a gradient that becomes evident at 9–12 hr APF. The timeline fits well with our previous finding that PN dendrites of different classes start segregating at around 6 hr APF, and specific targeting is evident at 12 hr APF (Jefferis et al., 2004). This observation suggests that specific dendritic targeting of PNs with different Sema-1a levels creates the gradient we observe at 16–18 hr APF; PNs expressing higher levels of Sema-1a target their dendrites to a progressively more DL region, thus creating a continuous Sema-1a gradient in the antennal lobe.

Loss of *sema-1a* Causes Direction-Specific Mistargeting of PN Dendrites

The correlation of Sema-1a expression levels and dendritic target positions (Figure 2), together with the cell-autonomous function of Sema-1a in PN axon targeting (Figure 1), raises the possibility that PNs use Sema-1a as a receptor to read spatial information along the DL-VM axis provided by an unidentified ligand(s). The level of Sema-1a signaling would thus instruct positioning of PN dendrites along this axis. This hypothesis predicts that dendrites of a *sema-1a* mutant PN that normally targets to the DL region should mistarget in the VM direction. We tested this prediction by performing single cell loss-of-function MARCM analyses for four PN classes (DL1, DA1, DC3, and VM2) using the null allele *sema-1a*^{P1}. Our choice of PN classes is limited by the availability of Gal4 lines that allow us to identify PN classes independent of dendritic targeting. Nevertheless, these four classes cover a large range along the DL-VM axis, thereby sampling different locations along the Sema-1a gradient (Figure 3A).

In accordance with our prediction, DL1 PN dendrites that normally target the most DL glomerulus exhibited severe VM mistargeting, sometimes targeting outside the antennal lobe (Figure 3B, arrows). A quantitative analysis of dendrite distributions along the DL-VM axis (orange arrow in Figure 3A; details described in Figure S1) confirmed this observation (Figure 3F). DA1 PNs that normally target less dorsolaterally than DL1 (especially during early pupal development; data not shown) also showed significant mistargeting in the VM direction, although to a lesser extent (Figure 3C, arrows; Figure 3F). Centrally targeting DC3 PNs in *sema-1a*$^{-/-}$ single cell clones showed a mild but statistically significant shift in the VM direction (Figures 3D and 3F). Ventromedially targeting VM2 PNs still targeted most of their dendrites to the appropriate area despite the lack of Sema-1a (Figures 3E and 3F). In addition to these phenotypes, we observed broadening of dendritic fields in several clones. This may be a response of dendrites when they lack correct targeting information (see Discussion).

Without the knowledge of the ligand source and distribution, it is unclear whether mistargeting inside and outside the antennal lobe should be treated as spatially continuous phenotypes. Therefore, as a conservative approach, we also quantified dendritic distributions only inside the antennal lobe, excluding mistargeting outside the antennal lobe (e.g., bottom arrows in Figure 3B,

is plotted for WT (blue) and *sema-1a*$^{-/-}$ (red). The mean position for each clone is calculated, and the numbers at the bottom of each graph represent the mean of mean positions (indicated by the dotted lines) ± SEM for all samples of the same condition. DL1 WT: n = 10, DL1 *sema-1a*$^{-/-}$: n = 11, $p < 0.001$ (***); DA1 WT: n = 10, DA1 *sema-1a*$^{-/-}$: n = 10, $p < 0.01$ (**); DC3 WT: n = 12, DC3 *sema-1a*$^{-/-}$: n = 10, $p < 0.05$ (*); VM2 WT: n = 10, VM2 *sema-1a*$^{-/-}$: n = 7, $p > 0.4$. These and following statistical analyses are by permutation tests, 100,000 repetitions.

(G) Quantification of dendritic distributions within the antennal lobe (excluding mistargeting outside) along the same DL-VM axis as in (F). WT versus *sema-1a*$^{-/-}$, DL1: $p < 0.001$; DA1: $p < 0.01$; DC3: $p < 0.05$; VM2: $p > 0.4$. n = 8 for DL1 *sema-1a*$^{-/-}$ (excluding three samples that target only outside the antennal lobe), and the data set for other genotypes is the same as in (F).

(H) Quantification of dendritic distributions along the orthogonal, VL-DM axis (the green axis in A) reveals no shift for all four classes examined. $p > 0.10$. The data set is the same as in (G). This quantification was done essentially identical to the quantification along the DL-VM axis, with bin1 being the most VL.

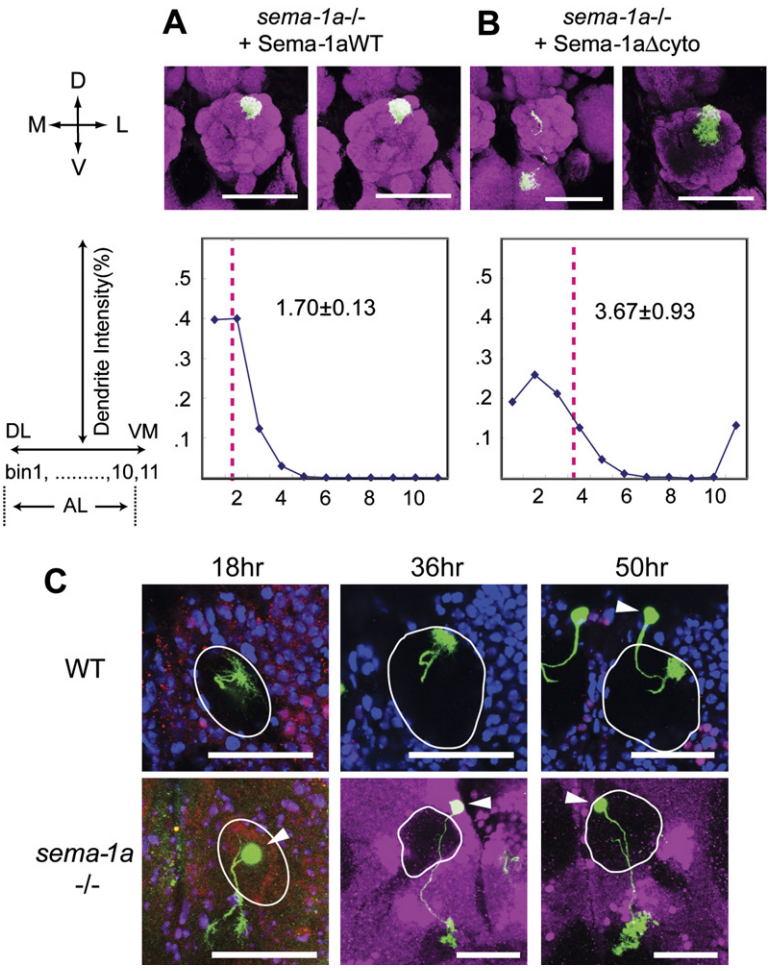

Figure 4. Cell-Autonomous and Early Requirement of Sema-1a in DL1 Dendritic Targeting

(A and B) The ventromedial mistargeting of *sema-1a*$^{-/-}$ DL1 PNs (Figure 3B) can be rescued by cell-autonomous expression of a full-length *sema-1a* transgene (A) (n = 8, p > 0.6 compared to wild-type), but not by expression of a cytoplamic deletion form of *sema-1a* (B) (n = 8, p > 0.08 compared to *sema-1a*$^{-/-}$). Quantification is as in Figure 3F. Statistics are by a permutation test, 100,000 repetitions.

(C) Ventromedial mistargeting of dendrites of *sema-1a*$^{-/-}$ DL1 PNs is observed at early developmental time points (left panel, 18 hr APF, n = 3/15; middle panel, 36 hr APF, n = 1/5; right panel, 50 hr APF, n = 1/5). We only quantified the most severe case of mistargeting out of the antennal lobe, which is unequivocal even at the earliest stage examined. Developing antennal lobes are outlined based on DAPI staining. Green: mCD8-GFP marking single-cell MARCM clones of DL1 PN; magenta: anti-Acj6; blue: DAPI. Arrowheads are PN cell bodies; in some brains they are anterior to the antennal lobe but in the 2D projections appear within the lobe.

All images are single-cell clones. Scale bar, 50 μm.

bottom left). This resulted in a similar trend (Figure 3G compared with 3F): from DL1, DA1, DC3, to VM2, there is a progressive decrease in the degree of *sema-1a*$^{-/-}$ PN dendritic mistargeting, with a corresponding increase of the p value when compared with control.

As another measure of severity of dendritic mistargeting in different PN classes, we quantified amounts of dendrites targeting the correct glomeruli defined solely by the nc82 staining. (The glomerular border of DC3 is difficult to identify with the nc82 staining, and therefore this class was excluded from this analysis.) As expected, wild-type PNs sent the vast majority of their dendrites to the correct glomeruli (90%, 91.5%, and 88% for DL1, DA1, and VM2, respectively). In contrast, *sema-1a*$^{-/-}$ clones sent smaller fractions of their total dendritic mass to the correct glomeruli (43%, 68%, and 77% for DL1, DA1, and VM2, respectively). DL1 is more severely affected by loss of *sema-1a* than DA1, which is in turn more severely affected than VM2. This analysis further supports the graded phenotypes of different PN classes along the Sema-1a gradient, with more dorsolaterally targeting PNs more severely affected.

To test whether dendritic mistargeting of *sema-1a*$^{-/-}$ PNs is direction-specific, we quantified dendritic distributions inside the antennal lobe along the VL-DM axis (green arrow in Figure 3A), orthogonal to the observed Sema-1a gradient in the DL-VM axis (Figure 2). We did not find a significant shift for any of the four classes examined (Figure 3H). These results strongly support the idea that Sema-1a directs dendritic targeting specifically along the DL-VM axis.

The DL1 dendritic mistargeting defects can be rescued by cell-autonomous expression of a full-length *sema-1a* transgene (Figure 4A), but not by expression of Sema-1a that lacks the cytoplasmic domain (Figure 4B). The expression level of transgenic Sema-1a could be higher than wild-type, but Sema-1a overexpression has no effect on this most DL-targeting class (data not shown). Localization of the Sema-1a$^{\Delta cyto}$ protein in the dendrites was confirmed by antibody staining (data not shown). Delayed expression onset of other Gal4 lines prevented us from performing the rescue experiment for other PN classes. At least for the DL1 class, therefore, Sema-1a acts as a receptor, or part of a receptor complex, in PN dendritic targeting.

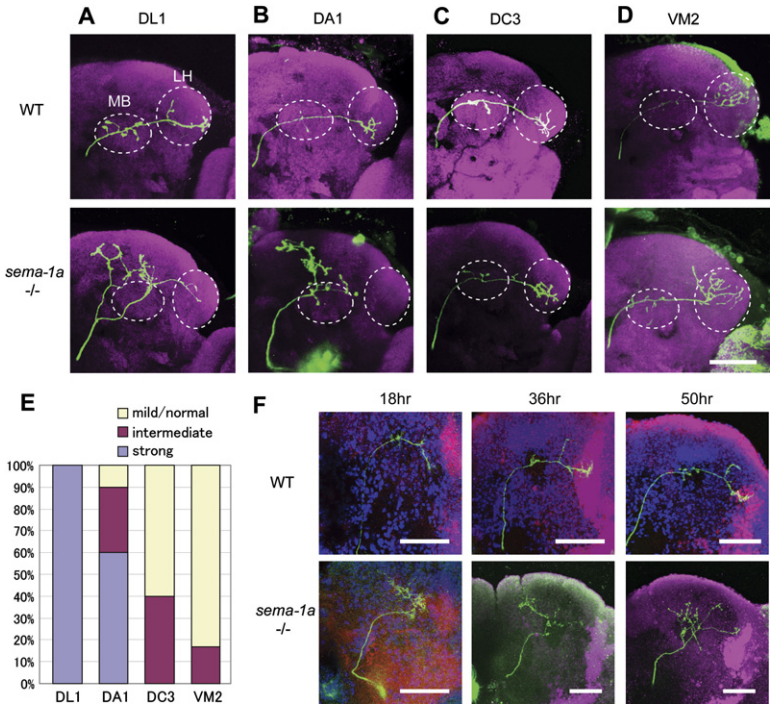

Figure 5. Axon Phenotypes of *sema-1a*$^{-/-}$ Single-Cell Clones

(A–D) DL1 (A) and DA1 (B) PN single-cell clones show severe mistargeting and overbranching phenotypes in *sema-1a*$^{-/-}$, while DC3 (C) and VM2 (D) PNs show only mild defects.

(E) Quantification of *sema-1a*$^{-/-}$ axon phenotypes. Strong: multiple branches mistargeting out of the correct route or target areas (dotted lines) with further overbranching; intermediate: few branches or one long branch mistargeting out of the correct route; mild/normal: all termini in correct target areas, or only one short branch out of the correct route or target areas. n = 14 for DL1, 10 for DA1, 10 for DC3, and 6 for VM2.

(F) Mistargeting of axons of *sema-1a*$^{-/-}$ DL1 PNs is observed at early developmental time points (left panel, 18 hr APF, n = 2/2; middle panel, 36 hr APF, n = 3/3; right panel, 50 hr APF, n = 2/2). Labeling is as in Figure 4C. Scale bar, 50 μm.

The VM mistargeting phenotype of the DL1 PN dendrites was observed at all developmental stages examined (18, 36, and 50 hr APF; Figure 4C). The earliest time point we examined was prior to the ORN axon invasion of the antennal lobe (Jefferis et al., 2004), indicating that Sema-1a acts in the initial, ORN-independent phase of dendritic targeting.

Sema-1a Is Differentially Required for Axon Targeting of Different PN Classes

As described above, DL1 PNs mutant for *sema-1a* show severe and 100% penetrant axon targeting defects, with axons misrouted dorsally (Figures 1B, 5A, and 5E). A similar mistargeting was observed for DA1 PN axons, although the penetrance and severity of the phenotypes were lower (Figures 5B and 5E). The axon-targeting defects for the DC3 and VM2 PNs were subtle and less penetrant (Figures 5C–5E). Thus, Sema-1a is differentially required not only for dendrite but also for axon targeting of different PN classes. The PN classes that target their dendrites more dorsolaterally in the antennal lobe have a higher dependence on Sema-1a for correct axon targeting, consistent with a higher level of Sema-1a expression in these PNs. By contrast, more ventromedial PNs express lower levels of Sema-1a, and their axon targeting is less dependent on Sema-1a.

The mistargeting of the DL1 PN was also observed at as early as 18 hr APF, when PN axons just start to elaborate their terminal arborization in the MB calyx and the lateral horn (Figure 5F), indicating that as in dendritic targeting (Figure 4C), Sema-1a acts at an early stage of axon targeting.

Overexpression of Sema-1a Shifts PN Dendrites Dorsolaterally in a Dose-Dependent Manner

If the level of Sema-1a plays an instructive role in PN dendritic targeting, overexpression of Sema-1a should cause a DL shift of PN dendrites. To test this prediction, we overexpressed Sema-1a only in labeled PNs using the MARCM system. PN neuroblast clones overexpressing Sema-1a failed to innervate their normal VM target glomeruli; instead, their dendrites shifted to the DL region of the antennal lobe (Figure 6). This effect is dose sensitive: Sema-1a expression from one copy of the transgene did not result in a significant shift (Figure 6B), whereas expression from two copies of the transgene did. (We have found that the level of overexpression from one copy of the transgene was low and that from two copies was much higher; see Experimental Procedures.) Moreover, this overexpression phenotype was stronger when flies were reared at 25°C compared to 18°C (Figures 6C and 6D), due to increased Gal4-UAS activity at the higher temperature. Finally, raising the flies in the presence of tub-Gal80^{ts}, a temperature-sensitive form of the Gal4 inhibitor (McGuire et al., 2004), at a permissive temperature during development completely suppressed this overexpression phenotype (Figure 6E). Thus, Sema-1a overexpression during development shifts the dendritic targeting dorsolaterally in a dose-dependent manner.

The overexpression effect was also specific to the DL-VM axis. Quantification of dendritic distrubitions along the VL-DM axis did not reveal a significant shift for any of the experimental conditions (wild-type: 5.72 ± 0.05; one-copy overexpression: 5.76 ± 0.06; two-copy overexpression at 18°C: 5.81 ± 0.11; two-copy overexpression at

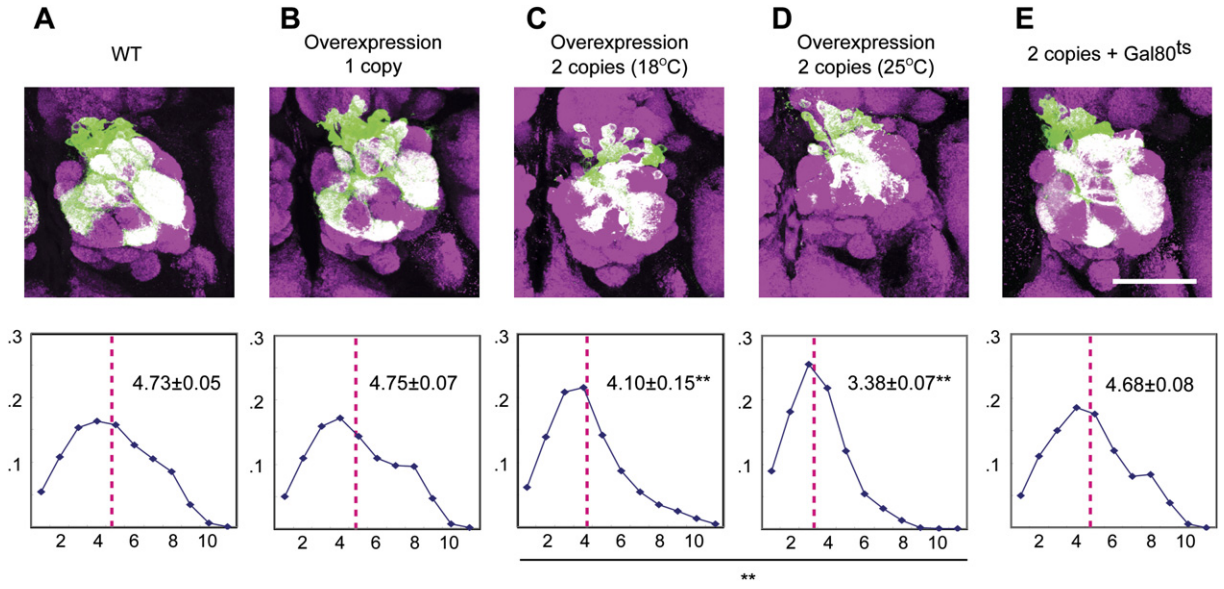

Figure 6. Effect of Sema-1a Overexpression on PN Dendritic Targeting

(A) PNs derived from an anterodorsal neuroblast MARCM clone innervate a stereotypic set of glomeruli in WT (n = 25).

(B) One copy of Sema-1a transgene expression in the anterodorsal neuroblast MARCM clones does not cause a significant effect (25°C, n = 16, p = 0.37 compared with WT).

(C and D) Two copies of transgene expression results in a significant dorsolateral shift of the dendritic field (in C, 18°C, n = 32, $p < 0.01$; in D, 25°C, n = 33, $p < 0.01$; both compared with WT). The higher overexpression has a stronger effect than the lower overexpression (C versus D, $p < 0.01$).

(E) Rearing flies with tubP-Gal80^{ts} at a permissive temperature for Gal80 (18°C) suppressed the overexpression phenotype of two copies of Sema-1a (n = 14, p = 0.34 compared with WT).

Quantification is as in Figure 3. Green labeling dorsal to the antennal lobes is PN cell bodies and was not included in the quantifications. Overlap of green-labeled (CD8-GFP) dendrites and nc82 (magenta) appears white. Scale bar, 50 μm.

25°C: 6.17 ± 0.08; Gal80^{ts} control: 5.59 ± 0.05; $p > 0.05$ when each condition is compared with wild-type).

Taking together the expression study and loss- and gain-of-function analyses, we conclude that Sema-1a levels cell-autonomously direct PN dendritic targeting in the antennal lobe along the DL-VM axis (Figure 7, see Discussion).

DISCUSSION

Gradients and Discrete Neural Maps

Gradients of axon guidance molecules have been proposed almost half a century ago (Sperry, 1963) to specify neuronal connections and have since been identified in several systems. Graded Ephrin/Eph signaling plays crucial roles in instructing axon targeting of retinal ganglion cells in the tectum/superior colliculus in vertebrates (Cheng et al., 1995; Drescher et al., 1995; Brown et al., 2000; Hindges et al., 2002; Mann et al., 2002; Schmitt et al., 2006). Gradients of other molecules such as Wnt3 (Schmitt et al., 2006), Engrailed-2 (Brunet et al., 2005), and RGM/Neogenin (Monnier et al., 2002; Rajagopalan et al., 2004) have also been implicated in this process. Furthermore, gradients of Eph/Ephrin are essential in establishing the somatosensory thalamocortical projections (Vanderhaeghen et al., 2000; Dufour et al., 2003) and perhaps also the auditory map (Cramer, 2005). A primary feature shared by these systems is a continuous, topographic representation of sensory inputs: neighboring neurons target their axons to neighboring positions. Smooth gradients could thereby instruct the formation of such continuous maps.

By contrast, the olfactory system is organized in a qualitatively different way: ORNs project their axons, and second-order neurons project their dendrites, to discrete glomerular units. Cell-body positions do not predict the precise locations of their projections. ORNs whose cell bodies are dispersed in sensory epithelia converge their axons to single glomeruli (reviewed in Axel, 1995; Komiyama and Luo, 2006). Similarly, there is no correlation in positions of cell bodies and target glomeruli of second-order PNs in *Drosophila* (Jefferis et al., 2001). However, we show here that graded expression of a guidance molecule is still utilized for the formation of such a discrete sensory map. Our findings extend the importance of molecular gradients to the formation of discrete neural maps. This appears to be a general mechanism by which organisms utilize a limited number of genes to specify the vast number of connections necessary to construct a functional nervous system.

We provide definitive evidence that Sema-1a functions cell-autonomously in PNs for their dendritic and axonal

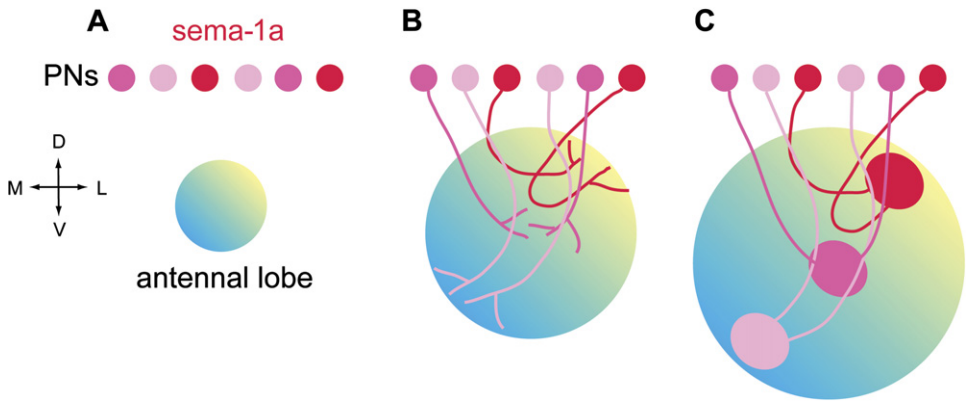

Figure 7. A Model for PN Dendritic Targeting

(A) Individual classes of PNs express different levels of Sema-1a (red), and the antennal lobe contains spatial information along the DL-VM axis (symbolized as the yellow-blue gradient as a possible scenario, analogous to the visual system).

(B) Graded Sema-1a expression directs the initial dendritic targeting: PNs expressing higher levels of Sema-1a target to more DL regions, while low expressers target the VM regions.

(C) At a later stage, the coarse targeting directed by Sema-1a (and additional positional cues in this and other axes) is refined through cell-cell interactions, including dendrite-dendrite interactions among PNs and axon-dendrite interactions between ORNs and PNs.

targeting. This function requires the cytoplasmic domain. Since deletion of the Sema-1a cytoplasmic domain does not affect its localization, the cytoplasmic domain could mediate signaling directly by interacting with intracellular proteins, or it could mediate interactions of Sema-1a with an essential coreceptor.

We propose that Sema-1a levels cell-autonomously direct initial PN targeting in the antennal lobe along the DL-VM axis (Figure 7). In one possible model, PNs with different Sema-1a levels—specified transcriptionally, posttranscriptionally or both—respond to a ligand gradient expressed along the same DL-VM axis (Figure 7A) by targeting their dendrites to different positions along this axis (Figure 7B). However, our data do not exclude other possibilities. For example, spatial information read by Sema-1a could be provided by a discrete combinatorial code of molecules. Future identification of the Sema-1a ligand and its cellular source and distribution will provide further insights as to how wiring specificity of the olfactory circuit originates.

Our mutant analyses indicate that Sema-1a signaling does not provide the single instructive force along the DL-VM axis. For example, *sema-1a*$^{-/-}$ PNs of all four classes analyzed retain preferences to occupy the correct glomeruli. In addition, interestingly, three out of seven *sema-1a*$^{-/-}$ VM2 mutant PNs showed subtle dendritic mistargeting in the DL direction (arrowhead in Figure 3E), which was never observed in wild-type controls. These observations are reminiscent of the mutant phenotypes of Ephrin-As (Feldheim et al., 2000) and EphBs (Hindges et al., 2002) in retinotopic mapping and suggest the presence of other forces instructing PN positioning along the DL-VM axis. This is expected, since a single, unidirectional force would cause all PN dendrites to target one corner of the antennal lobe. Sema-1a itself could act as a bidirectional receptor by switching its direction of responses in a concentration-dependent manner, as proposed for Ephrin-As (Hansen et al., 2004) and Ephrin-B1 (McLaughlin et al., 2003). Furthermore, other counterbalancing gradients, as proposed in the visual system by Wnt3 signaling (Schmitt et al., 2006), might work together with Sema-1a in specifying DL-VM positions of PN dendrites.

How could a continuous gradient be used to instruct the formation of a discrete map? We have found that graded expression of Sema-1a is required for initial targeting of PN dendrites (Figure 4C). We propose that this initial targeting is later refined through intercellular interactions that sharpen boundaries between glomeruli (Figure 7C). Indeed, dendrite-dendrite interactions among PNs mediated by the cell-adhesion molecule N-cadherin contribute to the refinement of PN dendritic targeting (Zhu and Luo, 2004). Interactions between ORN axons and their partner PN dendrites are likely to further sharpen glomerular boundaries and increase the fidelity of pre- and postsynaptic matching (Zhu et al., 2006). Broadening of dendritic fields observed in several mutant clones might indicate that these refinement processes are dependent on initial targeting; mistargeted dendrites may not be properly refined to achieve tight clustering normally observed within single glomeruli.

A similar developmental logic might be used in other systems, notably the convergent, discrete axon targeting of olfactory receptor neurons. In mice, OR expression areas in the olfactory epithelium form a continuous gradient, and the expression area of an OR along the dorsomedial-ventrolateral axis in the epithelium is tightly correlated with the position of axonal convergence in the olfactory bulb along the dorsal-ventral axis (Miyamichi et al., 2005). Thus, it is plausible that ORN axon targeting along

this axis is controlled by gradients of guidance molecules, such that ORNs express different levels of guidance receptors along the dorsomedial-ventrolateral axis in the epithelium, and differentially respond to their ligand gradients along the dorsal-ventral axis in the bulb. Indeed, several molecules have been shown to be expressed in gradients in the mouse olfactory system (Norlin et al., 2001). A recent study proposes that levels of G protein and cAMP signaling in ORNs determined by the basal activity of different ORs may instruct ORN axon targeting along the anterior-posterior axis of the olfactory bulb, through transcriptional regulation of axon-guidance molecules including neuropilin1 (Imai et al., 2006). Similar to our model of PN dendritic targeting, coarse targeting of ORN axons instructed by gradients could be refined through axon-axon interactions, which have been implicated in both flies (Komiyama et al., 2004; Sweeney et al., 2007) and mice (Ebrahimi and Chess, 2000; Feinstein and Mombaerts, 2004; Serizawa et al., 2006).

Coordination of Dendrite and Axon Targeting of the Same Neuron

Nervous systems are composed mostly of interneurons such as PNs. They face the challenging task of coordinating targeting specificity of their dendrites in the receiving end of information, and axons in the sending end, of the same neurons. This is essential for them to receive input from appropriate presynaptic neurons and relay information to appropriate postsynaptic neurons. In *Drosophila* PNs, for instance, the axon-targeting patterns in the higher olfactory centers are highly stereotyped according to their glomerular classes (defined by PN dendritic targets) (Marin et al., 2002; Wong et al., 2002). Compared to mechanisms of axon guidance and targeting, relatively little is known about mechanisms of dendrite guidance and targeting (reviewed in Jan and Jan, 2003), or the coordination of axonal and dendritic targeting specificity of the same neuron.

We previously showed that a pair of POU transcription factors plays a role in both PN dendritic and axonal targeting (Komiyama et al., 2003). Here we find that PNs whose dendrites target more dorsolaterally have a higher level of Sema-1a expression and are more dependent on Sema-1a for targeting of both axons and dendrites. We believe that Sema-1a regulates axon and dendrite targeting locally and independently, since these processes occur simultaneously (Jefferis et al., 2004), and we did not find correlation between severity of dendritic and axonal phenotypes within the same PN under the conditions when these phenotypes are partially penetrant (data not shown). Use of the same molecules to specify targeting of both axons and dendrites may help neurons to coordinate their input and output and at the same time reduce the number of molecules required for wiring the nervous system. Such dual functions of guidance molecules within single neurons (e.g., this study; Polleux et al., 2000) may be widely used in developing nervous systems.

As another example of economy and pleiotropy of guidance molecules, we found that Sema-1a also acts in ORNs for their axon targeting. In contrast to its cell-autonomous function in PNs described here, at a later stage of development, Sema-1a acts as a ligand for PlexinA to mediate ORN axon-axon interactions (Sweeney et al., 2007).

EXPERIMENTAL PROCEDURES

Mosaic Analyses

Mosaic analyses using MARCM for DL1 single-cell clones and neuroblast clones were performed as described (Komiyama et al., 2003). To generate DA1, DC3, and VM2 clones, flies of the following genotypes were heat shocked for 1.5 hr at variable times between 26–74 hr after larval hatching. (1) DA1 and DC3, wild-type control: *hsFlp*, *UAS-mCD8-GFP/+*; *Mz19-Gal4*, *FRT40A/ tubP-Gal80*, *FRT40A*. (2) DA1 and DC3, *sema-1a*$^{-/-}$: *hsFlp*, *UAS-mCD8-GFP/+*; *sema-1a*^{P1}, *Mz19-Gal4*, *FRT40A/ tubP-Gal80*, *FRT40A*. (3) VM2, wild-type control: *hsFlp*, *UAS-mCD8-GFP/NP5103*; *FRT40A/ tubP-Gal80*, *FRT40A*. (4) VM2 *sema-1a*$^{-/-}$: *hsFlp, UAS-mCD8-GFP/NP5103*; *sema-1a*^{P1}, *FRT40A/ tubP-Gal80*, *FRT40A*. For rescue experiments, the genotype was the following: *hsFlp*, *UAS-mCD8-GFP/+*; *sema-1a*^{P1}, *FRT40A/ tubP-Gal80*, *FRT40A*; *UAS-sema1a/+*. For overexpression experiments, the genotypes were the following: (1) one copy: *hsFlp*, *tubP-Gal80*, *FRT19A/ UAS-mCD8-GFP*, *FRT19A*; *GH146-Gal4*, *UAS-mCD8-GFP/ UAS-sema-1a.* (2) two copies: *hsFlp*, *UAS-mCD8-GFP/ +*; *tubP-Gal80*, *FRT40A*, *GH146-Gal4/ UAS-sema-1a, FRT40A*. (3) Gal80^{ts} suppression: *hsFlp*, *UAS-mCD8-GFP/ tubP-Gal80^{ts}*; *tubP-Gal80*, *FRT40A*, *GH146-Gal4/ UAS-sema-1a*, *FRT40A.* NP5103 (Tanaka et al., 2004) was obtained from the DGRC Kyoto Stock Center. MARCM clones for MB α'/β' neurons were generated by inducing clones at 72–96 hr after larval hatching in animals of the genotypes analogous to above, except that the MB OK107-Gal4 (Lee et al., 1999) was used instead of the PN Gal4s.

Immunofluorescence

Fixation, immunofluorescence, and imaging were performed as described (Komiyama et al., 2003) with the exception that some images were taken using Zeiss LSM 510. Rabbit anti-Sema-1a (kind gift of A. Kolodkin) was used at 1:2500. Rat anti-N-Cadherin (Developmental Studies Hybridoma Bank) was used at 1:30.

Quantification Procedures

For quantification of Sema-1a gradients at 16 hr APF, 11 antennal lobes stained for Sema-1a (9 of which costained for N-Cadherin) were randomly chosen and imaged using Zeiss LSM 510. A central confocal section was chosen from each brain, the DL-VM axis manually drawn, the antennal lobe was binned into five bins, and average fluorescence intensity in each bin was calculated. Values from different brains were normalized such that the average intensity from each brain was 100. For samples with N-Cadherin staining, the Sema-1a pattern and the N-Cadherin pattern were both analyzed in the same confocal section along the same DL-VM axis. Quantifications of Sema-1a gradients at earlier developmental stages were similarly performed.

Quantification of PN dendritic targeting positions is described in detail in Figure S1. Quantification of the fraction of dendrites targeting the correct glomeruli were performed by calculating the fluorescence intensity within a glomerulus whose border was manually drawn based solely on the nc82 staining, divided by the total fluorescence intensity.

Estimation of Sema-1a Overexpression Level in MARCM Neuroblast Clones

To estimate the MARCM overexpression level relative to endogenous Sema-1a (Figure 6), we generated a set of samples at 16 hr APF in which one antennal lobe has an anterodorsal neuroblast MARCM clone overexpressing Sema-1a and the contralateral antennal lobe

does not have a clone (as an internal control) and stained with anti-Sema-1a antibody. The mean intensities of top five confocal sections (1 micron step) of the antennal lobe, where the labeled dendrites are enriched, were calculated for both sides that were imaged at the same gain. (These sections also include dendrites of unlabeled PNs that do not overexpress Sema-1a.) We then calculated the ratios of mean fluorescence intensity of the clone-containing side over the control side for each brain. The geometric means are 1.25 for one copy (1.10, 1.16, 1.47, and 1.29 for four brains) and 3.03 for two copies (4.24, 3.64, 2.80, and 1.96 for four brains) of the transgene, respectively. This nonlinear increase from one copy (25% increase over the average Sema-1a endogenous level) to two copies (200% increase) may reflect a thresholding effect of Gal4 activity as the Gal80 concentration decreases after clone induction. The overexpression levels are likely lower at earlier time points during initial targeting and may explain the differential effect of one versus two copies of transgenes.

Supplemental Data

Supplemental Data include one figure and can be found with this article online at http://www.cell.com/cgi/content/full/128/2/399/DC1/.

ACKNOWLEDGMENTS

We thank A. Kolodkin, R. Murphey, T. Godenschwege, A. Couto, B. Dickson, E. Buchner, the Developmental Studies Hybridoma Bank, and the Bloomington and the DGRC Kyoto Stock Centers for reagents; B. Dickson, T. Clandinin, S. McConnell, K. Shen, R. Friedel, D. Manoli, and members of the Luo lab, especially B. Tasic, for comments and discussions; and A. Chau and M. Cohen for professional assistance in statistical analyses. This work was supported by fellowships from Japan Stanford Association (TK), Developmental and Neonatal Training Program (LS), EMBO (OS), and an NIH grant R01-DC005982 (LL). L.L. and K.C.G. are investigators of the Howard Hughes Medical Institute.

Received: July 1, 2006
Revised: November 10, 2006
Accepted: December 29, 2006
Published: January 25, 2007

REFERENCES

Axel, R. (1995). The molecular logic of smell. Sci. Am. *273*, 154–159.

Brown, A., Yates, P.A., Burrola, P., Ortuno, D., Vaidya, A., Jessell, T.M., Pfaff, S.L., O'Leary, D.D., and Lemke, G. (2000). Topographic mapping from the retina to the midbrain is controlled by relative but not absolute levels of EphA receptor signaling. Cell *102*, 77–88.

Brunet, I., Weinl, C., Piper, M., Trembleau, A., Volovitch, M., Harris, W., Prochiantz, A., and Holt, C. (2005). The transcription factor Engrailed-2 guides retinal axons. Nature *438*, 94–98.

Cafferty, P., Yu, L., Long, H., and Rao, Y. (2006). Semaphorin-1a functions as a guidance receptor in the Drosophila visual system. J. Neurosci. *26*, 3999–4003.

Cheng, H.J., Nakamoto, M., Bergemann, A.D., and Flanagan, J.G. (1995). Complementary gradients in expression and binding of ELF-1 and Mek4 in development of the topographic retinotectal projection map. Cell *82*, 371–381.

Couto, A., Alenius, M., and Dickson, B.J. (2005). Molecular, anatomical, and functional organization of the Drosophila olfactory system. Curr. Biol. *15*, 1535–1547.

Cramer, K.S. (2005). Eph proteins and the assembly of auditory circuits. Hear. Res. *206*, 42–51.

Dickson, B.J. (2002). Molecular mechanisms of axon guidance. Science *298*, 1959–1964.

Drescher, U., Kremoser, C., Handwerker, C., Loschinger, J., Noda, M., and Bonhoeffer, F. (1995). In vitro guidance of retinal ganglion cell axons by RAGS, a 25 kDa tectal protein related to ligands for Eph receptor tyrosine kinases. Cell *82*, 359–370.

Dufour, A., Seibt, J., Passante, L., Depaepe, V., Ciossek, T., Frisen, J., Kullander, K., Flanagan, J.G., Polleux, F., and Vanderhaeghen, P. (2003). Area specificity and topography of thalamocortical projections are controlled by ephrin/Eph genes. Neuron *39*, 453–465.

Ebrahimi, F.A., and Chess, A. (2000). Olfactory neurons are interdependent in maintaining axonal projections. Curr. Biol. *10*, 219–222.

Eckhardt, F., Behar, O., Calautti, E., Yonezawa, K., Nishimoto, I.I., and Fishman, M.C. (1997). A novel transmembrane semaphorin can bind c-src. Mol. Cell. Neurosci. *9*, 409–419.

Feinstein, P., and Mombaerts, P. (2004). A contextual model for axonal sorting into glomeruli in the mouse olfactory system. Cell *117*, 817–831.

Feldheim, D.A., Kim, Y.I., Bergemann, A.D., Frisen, J., Barbacid, M., and Flanagan, J.G. (2000). Genetic analysis of ephrin-A2 and ephrin-A5 shows their requirement in multiple aspects of retinocollicular mapping. Neuron *25*, 563–574.

Fishilevich, E., and Vosshall, L.B. (2005). Genetic and functional subdivision of the Drosophila antennal lobe. Curr. Biol. *15*, 1548–1553.

Flanagan, J.G. (2006). Neural map specification by gradients. Curr. Opin. Neurobiol. *16*, 59–66.

Godenschwege, T.A., Hu, H., Shan-Crofts, X., Goodman, C.S., and Murphey, R.K. (2002). Bi-directional signaling by Semaphorin 1a during central synapse formation in Drosophila. Nat. Neurosci. *5*, 1294–1301.

Hansen, M.J., Dallal, G.E., and Flanagan, J.G. (2004). Retinal axon response to ephrin-as shows a graded, concentration-dependent transition from growth promotion to inhibition. Neuron *42*, 717–730.

Hindges, R., McLaughlin, T., Genoud, N., Henkemeyer, M., and O'Leary, D.D. (2002). EphB forward signaling controls directional branch extension and arborization required for dorsal-ventral retinotopic mapping. Neuron *35*, 475–487.

Imai, T., Suzuki, M., and Sakano, H. (2006). Odorant receptor-derived cAMP signals direct axonal targeting. Science *314*, 657–661.

Jan, Y.N., and Jan, L.Y. (2003). The control of dendrite development. Neuron *40*, 229–242.

Jefferis, G.S.X.E., Marin, E.C., Stocker, R.F., and Luo, L. (2001). Target neuron prespecification in the olfactory map of Drosophila. Nature *414*, 204–208.

Jefferis, G.S.X.E., Vyas, R.M., Berdnik, D., Ramaekers, A., Stocker, R.F., Tanaka, N., Ito, K., and Luo, L. (2004). Developmental origin of wiring specificity in the Olfactory System of *Drosophila*. Development *131*, 117–130.

Klostermann, A., Lutz, B., Gertler, F., and Behl, C. (2000). The orthologous human and murine semaphorin 6A-1 proteins (SEMA6A-1/Sema6A-1) bind to the enabled/vasodilator-stimulated phosphoprotein-like protein (EVL) via a novel carboxyl-terminal zyxin-like domain. J. Biol. Chem. *275*, 39647–39653.

Kolodkin, A.L., Matthes, D.J., and Goodman, C.S. (1993). The semaphorin genes encode a family of transmembrane and secreted growth cone guidance molecules. Cell *75*, 1389–1399.

Komiyama, T., Johnson, W.A., Luo, L., and Jefferis, G.S.X.E. (2003). From lineage to wiring specificity. POU domain transcription factors control precise connections of Drosophila olfactory projection neurons. Cell *112*, 157–167.

Komiyama, T., Carlson, J.R., and Luo, L. (2004). Olfactory receptor neuron axon targeting: intrinsic transcriptional control and hierarchical interactions. Nat. Neurosci. *7*, 819–825.

Komiyama, T., and Luo, L. (2006). Development of wiring specificity in the olfactory system. Curr. Opin. Neurobiol. *16*, 67–73.

Komiyama, T., and Luo, L. (2007). Intrinsic control of precise dendritic targeting of olfactory projection neurons by an ensemble of transcription factors. Curr. Biol., in press.

Kumanogoh, A., and Kikutani, H. (2004). Biological functions and signaling of a transmembrane semaphorin, CD100/Sema4D. Cell. Mol. Life Sci. *61*, 292–300.

Laissue, P.P., Reiter, C., Hiesinger, P.R., Halter, S., Fischbach, K.F., and Stocker, R.F. (1999). Three-dimensional reconstruction of the antennal lobe in Drosophila melanogaster. J. Comp. Neurol. *405*, 543–552.

Lee, T., and Luo, L. (1999). Mosaic analysis with a repressible cell marker for studies of gene function in neuronal morphogenesis. Neuron *22*, 451–461.

Lee, T., Lee, A., and Luo, L. (1999). Development of the Drosophila mushroom bodies: sequential generation of three distinct types of neurons from a neuroblast. Development *126*, 4065–4076.

Leighton, P.A., Mitchell, K.J., Goodrich, L.V., Lu, X., Pinson, K., Scherz, P., Skarnes, W.C., and Tessier-Lavigne, M. (2001). Defining brain wiring patterns and mechanisms through gene trapping in mice. Nature *410*, 174–179.

Mann, F., Ray, S., Harris, W., and Holt, C. (2002). Topographic mapping in dorsoventral axis of the Xenopus retinotectal system depends on signaling through ephrin-B ligands. Neuron *35*, 461–473.

Marin, E.C., Jefferis, G.S.X.E., Komiyama, T., Zhu, H., and Luo, L. (2002). Representation of the glomerular olfactory map in the Drosophila brain. Cell *109*, 243–255.

McGuire, S.E., Mao, Z., and Davis, R.L. (2004). Spatiotemporal gene expression targeting with the TARGET and gene-switch systems in Drosophila. Sci. STKE *220*, pl6.

McLaughlin, T., Hindges, R., Yates, P.A., and O'Leary, D.D. (2003). Bifunctional action of ephrin-B1 as a repellent and attractant to control bidirectional branch extension in dorsal-ventral retinotopic mapping. Development *130*, 2407–2418.

McLaughlin, T., and O'Leary, D.D. (2005). Molecular gradients and development of retinotopic maps. Annu. Rev. Neurosci. *28*, 327–355.

Miyamichi, K., Serizawa, S., Kimura, H.M., and Sakano, H. (2005). Continuous and overlapping expression domains of odorant receptor genes in the olfactory epithelium determine the dorsal/ventral positioning of glomeruli in the olfactory bulb. J. Neurosci. *25*, 3586–3592.

Monnier, P.P., Sierra, A., Macchi, P., Deitinghoff, L., Andersen, J.S., Mann, M., Flad, M., Hornberger, M.R., Stahl, B., Bonhoeffer, F., and Mueller, B.K. (2002). RGM is a repulsive guidance molecule for retinal axons. Nature *419*, 392–395.

Norlin, E.M., Alenius, M., Gussing, F., Hagglund, M., Vedin, V., and Bohm, S. (2001). Evidence for gradients of gene expression correlating with zonal topography of the olfactory sensory map. Mol. Cell. Neurosci. *18*, 283–295.

Polleux, F., Morrow, T., and Ghosh, A. (2000). Semaphorin 3A is a chemoattractant for cortical apical dendrites. Nature *404*, 567–573.

Rajagopalan, S., Deitinghoff, L., Davis, D., Conrad, S., Skutella, T., Chedotal, A., Mueller, B.K., and Strittmatter, S.M. (2004). Neogenin mediates the action of repulsive guidance molecule. Nat. Cell Biol. *6*, 756–762.

Schmitt, A.M., Shi, J., Wolf, A.M., Lu, C.C., King, L.A., and Zou, Y. (2006). Wnt-Ryk signalling mediates medial-lateral retinotectal topographic mapping. Nature *439*, 31–37.

Serizawa, S., Miyamichi, K., Takeuchi, H., Yamagishi, Y., Suzuki, M., and Sakano, H. (2006). A neuronal identity code for the odorant receptor-specific and activity-dependent axon sorting. Cell *127*, 1057–1069.

Sperry, R.W. (1963). Chemoaffinity in the orderly growth of nerve fiber patterns and connections. Proc. Natl. Acad. Sci. USA *50*, 703–710.

Stocker, R.F., Heimbeck, G., Gendre, N., and de Belle, J.S. (1997). Neuroblast ablation in Drosophila P[GAL4] lines reveals origins of olfactory interneurons. J. Neurobiol. *32*, 443–456.

Sweeney, L.B., Couto, A., Chou, Y.-H., Berdnik, D., Dickson, B.J., Luo, L., and Komiyama, T. (2007). Target restriction of olfactory receptor neurons by Semaphorin-1a/PlexinA mediated axon-axon interaction. Neuron *53*, 185–200.

Tanaka, N.K., Awasaki, T., Shimada, T., and Ito, K. (2004). Integration of chemosensory pathways in the Drosophila second-order olfactory centers. Curr. Biol. *14*, 449–457.

Toyofuku, T., Zhang, H., Kumanogoh, A., Takegahara, N., Yabuki, M., Harada, K., Hori, M., and Kikutani, H. (2004). Guidance of myocardial patterning in cardiac development by Sema6D reverse signalling. Nat. Cell Biol. *6*, 1204–1211.

Vanderhaeghen, P., Lu, Q., Prakash, N., Frisen, J., Walsh, C.A., Frostig, R.D., and Flanagan, J.G. (2000). A mapping label required for normal scale of body representation in the cortex. Nat. Neurosci. *3*, 358–365.

Winberg, M.L., Noordermeer, J.N., Tamagnone, L., Comoglio, P.M., Spriggs, M.K., Tessier-Lavigne, M., and Goodman, C.S. (1998). Plexin A is a neuronal semaphorin receptor that controls axon guidance. Cell *95*, 903–916.

Wong, A.M., Wang, J.W., and Axel, R. (2002). Spatial representation of the glomerular map in the Drosophila protocerebrum. Cell *109*, 229–241.

Yu, H.H., Araj, H.H., Ralls, S.A., and Kolodkin, A.L. (1998). The transmembrane Semaphorin Sema I is required in Drosophila for embryonic motor and CNS axon guidance. Neuron *20*, 207–220.

Zhu, H., Hummel, T., Clemens, J.C., Berdnik, D., Zipursky, S.L., and Luo, L. (2006). Dendritic patterning by Dscam and synaptic partner matching in the Drosophila antennal lobe. Nat. Neurosci. *3*, 349–355.

Zhu, H., and Luo, L. (2004). Diverse functions of N-cadherin in dendritic and axonal terminal arborization of olfactory projection neurons. Neuron *42*, 63–75.